NANO LETTERS

Letter

pubs.acs.org/NanoLett

Nano-Optical Conveyor Belt, Part II: Demonstration of Handoff Between Near-Field Optical Traps

Yuxin Zheng,*[,†] Jason Ryan,*[,†] Paul Hansen,[‡] Yao-Te Cheng,[§] Tsung-Ju Lu,[∥] and Lambertus Hesselink[†,‡]

[†]Department of Electrical Engineering, [‡]Department of Applied Physics, and [§]Department of Materials Science and Engineering, Stanford University, Stanford, California 94305, United States

[∥]Department of Electrical Engineering, Massachusetts Institute of Technology, Cambridge, Massachusetts 02139, United States

ABSTRACT: Optical tweezers have been widely used to manipulate biological and colloidal material, but the diffraction limit of far-field optics makes focused beams unsuitable for manipulating nanoscale objects with dimensions much smaller than the wavelength of light. While plasmonic structures have recently been successful in trapping nanoscale objects with high positioning accuracy, using such structures for manipulation over longer range has remained a significant challenge. In this work, we introduce a conveyor belt design based on a novel plasmonic structure, the resonant C-shaped engraving (CSE). We show how long-range manipulation is made possible by means of handoff between neighboring CSEs, and we present a simple technique for controlling handoff by rotating the polarization of laser illumination. We experimentally demonstrate handoff between a pair of CSEs for polystyrene spheres 200, 390, and 500 nm in diameter. We then extend this technique and demonstrate controlled particle transport down a 4.5 μm long "nano-optical conveyor belt."

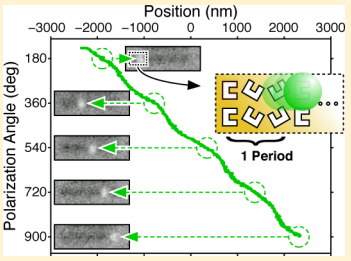

KEYWORDS: *Plasmonic antenna, optical tweezer, C-shaped engraving, near-field, handoff, conveyor belt*

Conventional optical tweezers have found numerous applications in biology,[1−6] soft condensed matter physics,[7−10] and "lab-on-a-chip" technology.[11−14] However, the diffraction limit of far-field optics sets an upper bound on the electric field intensity gradient for a given optical power, intrisically limiting our ability to capture and position nanoscale objects. In recent years, optical trapping of single nano-objects has also been achieved with optical near-fields from plasmonic antennas and apertures.[15−19] These resonant devices produce extraordinary concentrations of field energy in deeply subwavelength-size spots, providing the high field intensity gradients necessary for nanometric trapping under much lower optical power. Yet the optical near-field of a localized plasmonic resonator exists only near the resonator's surface. This fact limits the application of near-field trapping forces to a resonator's immediate vicinity, restricting the range over which small objects may be moved. Indeed, while rotation of single nanoparticles around single resonating gold pillars has been demonstrated by Wang and collegues,[19] controlled transport over longer range has remained a considerable challenge.

Recently, Hansen et al.[20] have proposed a nano-optical conveyor design to address this challenge. The design consists of a linear repeating structure of three distinct optical traps produced by resonating structures such as C-shaped apertures,[21] each element separately addressable by its resonant wavelength or polarization. By exciting each of the three sets of traps in a periodic sequence, nanoparticles can be handed off between adjacent traps and peristaltically drawn down a track of arbitrary length. Such nano-optical conveyors can be designed to bear trapped objects along paths of any direction and shape without using complicated beam shaping optics.

In this paper, we describe the first experimental demonstration of this idea. Previously suggested C-aperture based designs performed less well than expected because the aperture edges impede particle movement and because the metal membrane's poor capacity for thermal dissipation resulted in significant temperature rise. To overcome these issues, we replaced the aperture with a shallow C-shaped depression, the CSE, which can be easily integrated with a heat sink. In addition, the CSE can be filled with dielectric to planarize the surface and promote smooth particle motion. Because the key function of our scheme is handoff between adjacent traps, we first present in detail the theoretical design and the experimental results for nanoparticle handoff between just two traps. We then demonstrate a near-field optical conveyor 4.5 μm in length that we operate by continuously rotating the polarization of illumination.

We begin by examining the properties of a single resonant C-Shaped Engraving (CSE) in gold, the fundamental building block of our trapping system. The geometry and simulation results are shown in Figure 1 for a CSE tuned to operate with 1064 nm wavelength illumination. Finite-element method (FEM) field simulations using COMSOL software confirm that the CSE has a strong optical resonance that depends not only on wavelength but also on polarization angle. When illuminated with x-polarized light at the resonant wavelength,

Received: October 26, 2013
Revised: January 30, 2014
Published: May 7, 2014

dx.doi.org/10.1021/nl404045n | *Nano Lett.* 2014, 14, 2971−2976

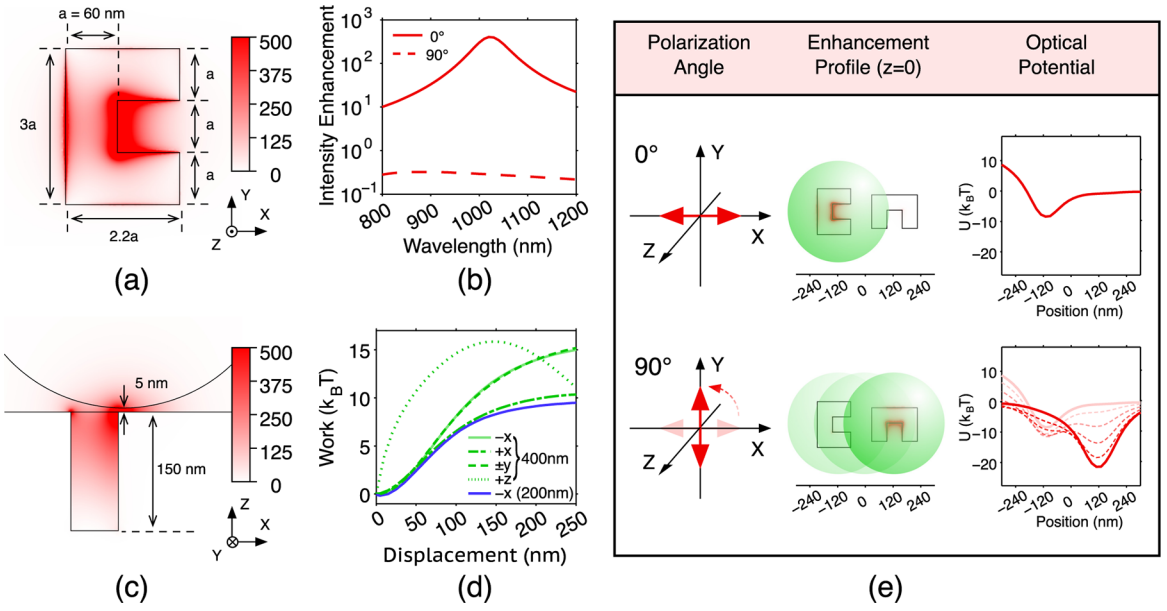

Figure 1. (a) Electric-field intensity enhancement on gold surface for a C-shaped engraving excited by 1064 nm illumination polarized along the *x*-axis. (b) Intensity enhancement measured at a point 10 nm above engraving ridge versus wavelength for illumination polarized along the *x*-axis (solid line) and *y*-axis (dotted line). (c) A polystyrene sphere near equilibrium, 5 nm above the substrate surface. (d) Work done by displacing a sphere of two different sizes from the position shown in (c) along the *x*-, *y*-, and *z*- axes. Because of the asymmetry of the "C" shape, the potential profiles are different along different directions. (e) The *x*-scan of the potential profiles of the CSE pair for various angles of illumination polarization from 0° to 90°. Note that the profiles are different even for 0° and 90°, as the scans are along different directions with respect to the "C". Illumination intensity held at 1 mW/μm^2.

the CSE strongly amplifies the electric field intensity in a small region just above the engraving ridge, known as the near-field "hot spot". Conversely, when illuminated with *y*-polarized light, the hot spot intensity enhancement is 1000 times weaker due to the absence of any significant CSE resonance for light polarized along that axis. For a general linear polarization in the *xy*-plane, which makes an angle θ to the *x*-axis, the resulting field is simply a linear combination of the fields produced by *x*- and *y*-polarized illumination due to the linearity of Maxwell's equations. Because the hot spot field intensity enhancement for *y*-polarization is very weak when compared with that for *x*-polarization, we may choose to neglect it in the field sum, and we can express the intensity enhancement approximately as

$$I_{\mathrm{enh}}(\theta) = \frac{|\mathbf{E}(0)\cos(\theta) + \mathbf{E}\left(\frac{\pi}{2}\right)\sin(\theta)|^2}{|\mathbf{E}_0|^2} \quad (1)$$

$$\approx I_{\mathrm{enh}}(0)\cos^2(\theta) \quad (2)$$

where $\mathbf{E}_0$ is the incident electric field. We calculate the optical force on a dielectric sphere near the hot spot for $\theta = 0$ by numerically integrating the flux of the Maxwell Stress Tensor over the sphere's outer surface, and we derive its potential energy from the force. As shown in Figure 1d, the hot spot of the CSE produces a deep potential well whose depth and size depends on the size of the sphere. As a rule of thumb, a larger sphere experiences a larger trap because it can be displaced further while still overlapping with the hot spot.

Rotating the polarization of illumination will transfer a trapped particle between two closely spaced CSEs that are rotationally offset. In order for handoff to be successful, the two traps need to be close enough, or the particle needs to be large enough, so that the particle overlaps the near field of both traps. Due to the traps' polarization sensitivity, rotating the angle of linear polarization changes the relative excitation of the traps. For simplicity, we first consider two engravings that are mutually perpendicular. As shown in Figure 1e, when we increase the polarization angle from 0° to 90° the trapping potential minimum shifts from left to right. Further increase of the polarization angle will then shift the potential minimum back to the left.

As can be inferred from the potential profiles, transfer of a sphere in such a manner from one trap to the next occurs in two stages. In the first stage, the original potential well becomes shallower while its minimum moves only slightly toward the neighboring trap. During this stage the particle stays in the original trap and slowly moves with the potential minimum position. Eventually, the energy barrier between the two wells becomes small enough to be overcome by thermal motion. In the second stage, the particle passes over this barrier and slides down into the adjacent well, completing the handoff process. The polarization angle at which the barrier is overcome by thermal motion depends on the temperature and the particular shape of the optical potential experienced by the particle.

The C-shaped engravings are fabricated using a poly(methyl methacrylate) (PMMA) template-stripping process.[22,23] First, a sacrificial layer of PMMA is coated onto a silicon wafer, followed by a layer of the negative-tone resist hydrogen silsesquioxane (HSQ). The engraving shapes are then defined as mesas in the HSQ using electron-beam lithography. After development, we coat 200 nm of gold, followed by 1000 nm of copper by sputtering deposition. The copper layer acts as a heat sink to minimize the temperature increase caused by Joule heating in the illuminated gold structures.[19] With this heat sink, our numerical simulations indicate a maximum temperature rise of 0.6 K under a Gaussian beam spot with a maximum power density of 1 mW/μm^2 and 3.5 μm 1/e^2 diameter, as is standard in our subsequent trapping experiments. A 10 mm × 10 mm

dx.doi.org/10.1021/nl404045n | *Nano Lett.* 2014, 14, 2971−2976

quartz slide is then glued onto the sample using UV adhesive (Norland Optical Adhesive 81) to form a structural backplate. Finally, the sample is released from the silicon substrate by dissolving the PMMA layer in an acetone bath. The HSQ remains inside the cavity of each engraving to provide a smooth surface for particle transport. Figure 2 shows the scanning

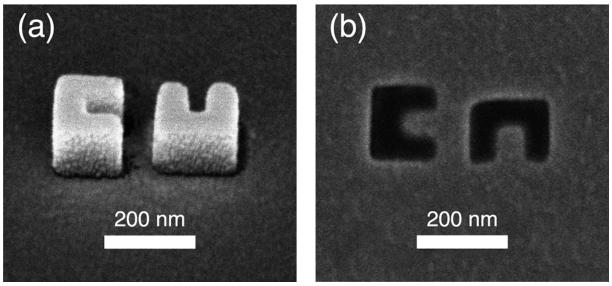

Figure 2. (a) SEM scan of HSQ mold after 5 nm of gold sputtering. (b) SEM scan of the final engraving pair in gold after release from the silicon substrate. HSQ remains inside the engravings, appearing as dark areas in the image.

electron microscope images of the mold formed by HSQ mesas and the final engraving pair after sample release. We have found that this method results in very smooth surfaces overall, as well as high quality shapes.

The schematic diagram of the optical setup is shown in Figure 3. The linearly polarized beam from a continuous wave Nd:YAG laser (λ_0 = 1064 nm) is weakly focused onto the sample using a 40× microscope objective (NA = 0.75) after passing through a beam contractor. Because the beam does not fill the entire input aperture of the objective, the beam experiences a reduced NA, resulting in a focused spot that has a $1/e^2$ diameter of 3.5 μm. Polarization rotation is achieved by

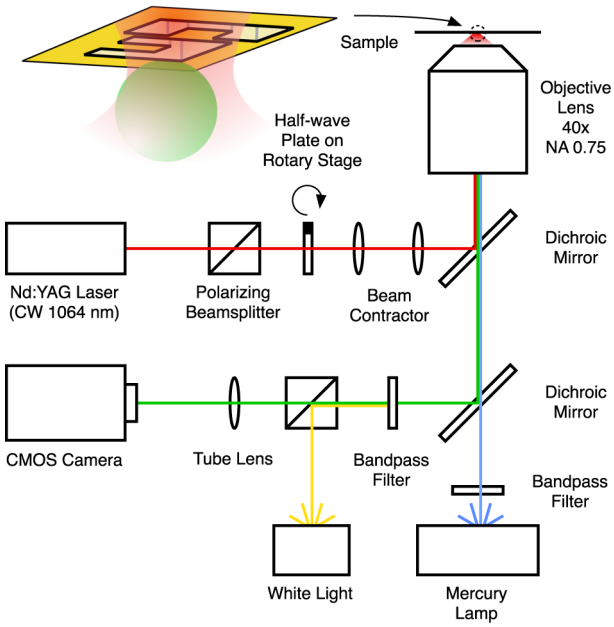

Figure 3. Schematic of the experimental apparatus. Both trapping and imaging are performed in reflection mode. The laser excites the engraving traps at 1064 nm. The mercury lamp excites fluorescence at 480 nm. A CMOS camera detects the fluorescent emission at 520 nm. An additional white light source provides brightfield illumination of the device surface.

rotating a half-wave plate in the beam path with a motorized rotary stage. Fluorescence imaging is performed using a Nikon Eclipse TE2000-U inverted fluorescence microscope. Another white light source is used for bright-field imaging. At the end of the imaging path, a monochrome CMOS camera (Thorlabs DCC1545M) is used to capture the video. Coordination of laser beam control with video recording is performed by a LabVIEW program that drives the laser power controller, rotary stage, and camera controls. Positions of the bead centers are calculated in each frame by performing a two-dimensional Gaussian fit of the intensity data in bright regions.

To prepare the sample, a small droplet of solution of fluorescent polystyrene spheres (Bangs Laboratories) is placed on a large coverslip, and the fabricated device chip is placed on top, spreading the solution underneath to form a fluid layer 10 μm in thickness. The fluid's low depth, together with the placement of heat-producing engravings on the ceiling of the chamber, serves to suppress thermal convection. A small amount of surfactant (5% by volume, Triton X-100) is added to the solution to minimize aggregation. Over the course of an experiment, the conventional trapping effect of the weakly focused laser can accumulate multiple beads whose overlapping images interfere with our measurement of particle trajectories. To avoid this, we dilute the bead solution and limit our study to the manipulation of one particle at a time.

We then perform trapping and handoff experiments for single polystyrene beads of various sizes (500, 390, and 200 nm in diameter) on CSE pairs with different spacings. The peak laser illumination intensity is set at 10 mW/μm^2, which draws beads toward the engraving pairs by conventional optical trapping and is seen to produce sufficiently stable near-field trapping on the surface of a CSE. During our experiments, we have also observed repulsion of particles from CSEs due to thermophoresis. However, this only appears to occur away from the engravings where the near-field optical forces are weaker than the thermal repelling force. Once a particle is close enough to an engraving, we observe that the optical force overcomes the thermal repelling force and forms a stable optical trap. Figure 4 shows the result of rotating the polarization from 0° to 90° for the three sphere sizes on a CSE pair with 310 nm spacing. In each case, rotation of the half wave plate causes the average x-position of the bead to shift from alignment with the left engraving to alignment with the right engraving. The

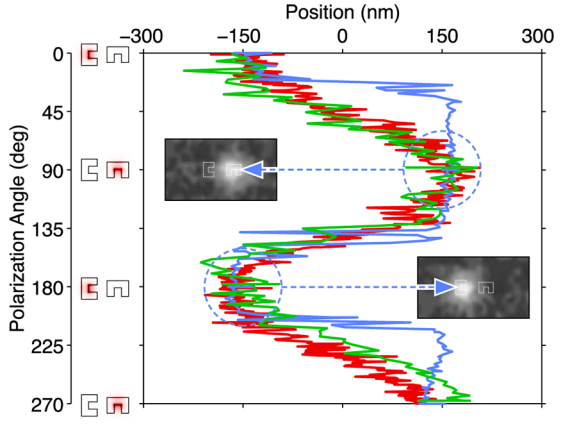

Figure 4. Handoff data for 500 nm (red line), 390 nm (green line), and 200 nm (blue line) spheres. Images inset show snapshots of the leftmost and rightmost positions of the 200 nm sphere.

dx.doi.org/10.1021/nl404045n | Nano Lett. 2014, 14, 2971−2976

average end point-to-end point bead displacement of 306 nm agrees very well with the center-to-center spacing of the engraving pair.

Notably, rotating the polarization slowly reveals the difference in the near-field potential landscape experienced by the different bead sizes. As shown in Figure 4, the large spheres translate smoothly while the small sphere undergoes a more discrete transition. The reason for this lies in the particle-near field overlap. The 500 and 390 nm spheres are large enough to overlap with the near field of both engravings at once, and the opposing trapping forces lower the potential barrier and shift the equilibrium position gradually as the polarization angle changes. On the other hand, the 200 nm spheres only overlap significantly with the near field of one engraving at a time. In this case, they tend to stay in one trap until the potential barrier between the two traps becomes shallow enough to allow a thermal transition. This particle size dependence of the potential landscape immediately suggests applications in nanoparticle sorting or filtering.[10]

Finally, the technique presented above is extended to perform three-phase manipulation, which enables continual translation. Using a periodic chain of three distinctly oriented CSEs (Figure 5), a controllable conveyor belt can be

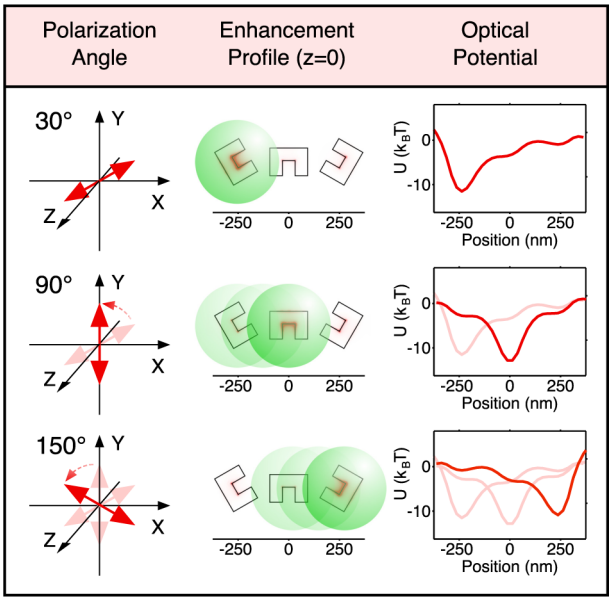

Figure 5. Beam polarized 30° to the *x*-axis excites the left engraving and traps a 400 nm polystyrene sphere. Rotation of polarization angle counterclockwise drives potential minimum to the right.

constructed.[20] In our experiments, we have successfully transported a 390 nm sphere on a double-rail conveyor design. The conveyor has 5 periods with axial and lateral spacings of d_x = 360 nm and d_y = 320 nm, respectively (Figure 6 inset). Our simulations suggest that a trapped sphere is expected to reside primarily over only one of the two rails at a time. Nevertheless, the overlap of the sphere with fields produced by the adjacent rail increases the total trapping force, which moderately deepens the total potential and adds a measure of robustness to manufacturing defects in the chain of engravings. To illuminate the entire 4.5 μm conveyor we increase the laser spot size to ~9 μm in diameter. The maximum illumination intensity at the center of the beam is 3.8 mW/μm^2. By uniformly rotating the polarization, we are able to move the sphere from one end

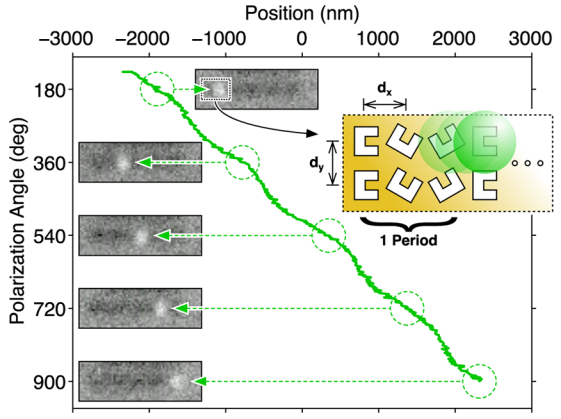

Figure 6. Position versus polarization angle for 390 nm bead. Images inset show snapshots of the sphere after each conveyor period. Schematic inset shows double-rail design.

of the conveyor belt to the other as seen in Figure 6. The inset snapshots show the displacement of the fluorescent sphere along the conveyor belt, which appears in the background as a dark, horizontal stripe. The particle motion is smooth and uniform with respect to polarization, suggesting good trapping and control capability. The slight undulation in the motion is because the trapping centers of CSEs of different orientations are not completely evenly distributed, as by our design. These undulations are clear evidence of the conveyor belt's periodic nature, as the number of ripples matches the number of periods in the conveyor.

While we have only demonstrated a relatively short linear conveyor belt and transported a single sphere in this paper, in principle the technology is scalable to handle a large number of particles in parallel and over a much longer distance. To transport more particles one would load the conveyor belt with multiple particles at different locations that correspond to the same conveyor belt phase. Because dielectric particles separated by at least one conveyor period interact with each other only weakly, they could be manipulated independently and simultaneously. To extend the conveyor range or to drive multiple conveyor belts, one would simply enlarge the illumination area while holding constant the level of power density. Consequently, the total amount of power required scales linearly with the total number of optical traps in the conveyor system.

As discussed in previous sections, the dynamics of particle handoff and transport depends on many parameters such as particle size, CSE spacing, illumination intensity, and polarization rotation speed. An accurate mechanical model requires numerically solving the Langevin equation over the full three-dimensional potential profile of the changing polarization. However, it is possible to obtain a quantitative estimate of some important performance parameters under reasonable assumptions. To simplify the analysis we will assume the case of the orthogonal CSE pair as shown in Figure 1e in the following calculations. Because the potential landscape induces a transition from stage one to stage two when the barrier turns into an inflection point, we denote the potential energy at this point as U_i, which itself is a function of particle diameter d, CSE spacing s, and is proportional to illumination power P. For slow operation in which thermal equilibrium is maintained throughout the process, we expect to first order approximation that the particle can be transferred successfully if the potential

dx.doi.org/10.1021/nl404045n | Nano Lett. 2014, 14, 2971−2976

depth at the transition point is larger than its random thermal kinetic energy E_k. In other words, if we set the zero point of potential energy at infinity ("far enough away" from the CSE), the condition for successful handoff is

$$E_{tot} = E_k + U_i(d, s, P) < 0 \quad (3)$$

Assuming a Maxwell−Boltzmann distribution of thermal energy, we may thus obtain over 95% probability of successful handoff if $U_i(d,s,P) < -4k_BT$. Given two of the three parameters d, s, and P, one can find the third in order for the conveyor to work at a desired reliability. Generally, the transfer is more reliable for smaller engraving spacings and larger particles because greater overlap results in stronger force from the adjacent trap. However, because the trap spacing is limited by both the physical and effective optical dimensions of each CSE, there is also a limit to the smallest particle that can be conveyed. It is possible to scale down the dimensions of each CSE by filling the engraving with a higher index dielectric material, but eventually scaling is limited by the skin depth of gold at the wavelength of operation and the degree to which interference can be tolerated between CSEs. Another concern is that more compact device configurations lead to intensified heating, which causes higher temperatures and stronger thermophoresis. Considering these limitations, we envision that this type of conveyor can potentially transport particles smaller than 100 nm in diameter with practical materials and optimized device configurations. Further study is needed to determine the ultimate limit of this type of near-field conveyor.

The maximum transport speed can also be estimated from the simulated potential/force profile. We ignore Brownian motion at this moment and assume an overdamped system so that the particle's instantaneous speed is $v = F/\beta$, where F is the position-dependent optical force and β is the viscous drag coefficient that depends on the sphere diameter, the viscosity of the fluid and the distance between the sphere and the surface.[2] Because the shift in the first stage of handoff is very small, we can ignore this stage and only calculate the time required for the particle to slip into the neighboring potential well. The time during which the particle moves from point a to point b can be calculated as $T = \int_{xa}^{xb}(1/v)dx = \beta \int_{xa}^{xb}(dx/F)$.

In slow operation mode, the particle is given enough time to move from the potential minimum of the left engraving at x_L to that of the right engraving at x_R as the polarization changes from 0° to 90°. In fast operation mode, the particle may be found to lag behind the potential oscillation such that it moves from $x_L - \Delta$ to $x_R - \Delta$ during the nominal handoff period. This is because the particle's speed becomes very low near the position of minimum potential where the force is close to zero. In order to find the maximum average speed, one can minimize the time to move one full trap spacing over the lag Δ as

$$T_{min} = \beta \min_{\Delta} \int_{x_L-\Delta}^{x_R-\Delta} \frac{dx}{F} \quad (4)$$

Thus, $f = 1/T_{min}$ corresponds to the maximum driving frequency such that the particle remains in phase with the conveyor excitation. Beyond this frequency, the particle cannot remain in phase and the transport speed begins to drop. With an engraving spacing of s, the maximum average transfer speed of the conveyor is thus $v_{max} = s/T_{min}$. For the design shown in Figure 1e, we find that v_{max} = 15 μm/s at 1 mW/μm^2 illumination. Because optical force scales with illumination intensity, we likewise expect the maximum transfer speed to scale with intensity until ohmic heating changes the viscous drag coefficient or other aspects of the fluidic environment.

To conclude, we have experimentally demonstrated the controlled handoff of single nanoparticles between orthogonal CSEs by polarization rotation and observed the particle size dependence of the handoff process. We have also demonstrated a 4.5 μm long near-field optical conveyor driven by polarization rotation. This was accomplished using low NA focusing objectives and without altering the intensity pattern of the beam in any way. The new device presented here opens the door to parallel manipulation of nano-objects in a form factor that is potentially very suitable for on-chip integration and thus may find many applications in routing, sorting and assembly of synthetic or biological nano-objects.

AUTHOR INFORMATION

Corresponding Authors

*E-mail: yuxinz@stanford.edu.

*E-mail: jason.ryan@stanford.edu.

Notes

The authors declare no competing financial interest.

ACKNOWLEDGMENTS

The authors would like to thank Professor Yuzuru Takashima at the University of Arizona for discussions on optical imaging, Mr. Karl Urbanek for assistance with high power lasers, and Max Yuen for discussions on Brownian motion. The authors send further thanks to Professor Kenneth Crozier at Harvard University for helpful discussions on optical trapping experiments. Funding was provided in part by the United States National Science Foundation (award number 1028372).

REFERENCES

(1) Ashkin, A.; Dziedzic, J. M. Optical Trapping and Manipulation Of Viruses and Bacteria. *Science* **1987**, *235*, 4795.

(2) Svoboda, K.; Block, S. M. Biological Applications of Optical Forces. *Annu. Rev. Biophys. Biomol. Struct.* **1994**, *23*, 247−285.

(3) Neuman, K.; Block, S. Optical Trapping. *Rev. Sci. Instrum.* **2004**, *75*, 2787.

(4) Fazal, F. M.; Block, S. M. Optical Tweezers Study Life Under Tension. *Nat. Photonics* **2011**, *5*, 318.

(5) Bockelmann, U.; Thomen, P.; Essevaz-Roulet, B.; Viasnoff, V.; Heslot, F. Unzipping DNA with Optical Tweezers: High Sequence Sensitivity and Force Flips. *Biophys. J.* **2002**, *82*, 1537−1553.

(6) Pang, Y.; Gordon, R. Optical Trapping of Single Protein. *Nano Lett.* **2012**, *12*, 402−406.

(7) Dholakia, K.; Čižmár, T. Shaping the Future of Manipulation. *Nat. Photonics* **2011**, *5*, 335−342.

(8) Grier, D. G.; Roichman, R. Holographic Optical Trapping. *Appl. Opt.* **2006**, *45*, 880−887.

(9) Korda, P. T.; Taylor, M. B.; Grier, D. G. Kinetically Locked-in Colloidal Transport in an Array of Optical Tweezers. *Phys. Rev. Lett.* **2002**, *89*, 128301.

(10) Pelton, M.; Ladavac, K.; Grier, D. G. Transport and Fractionation in Periodic Potential-energy Landscapes. *Phys. Rev. E* **2004**, *70*, 1−10.

(11) MacDonald, G. C.; Spalding, G. C.; Dholakia, K. Microfluidic Sorting in an Optical Lattice. *Nature* **2003**, *426*, 421−424.

(12) Eriksson, E.; Enger, J.; Nordlander, B.; Erjavec, N.; Ramser, K.; Goksor, M.; Hohmann, S.; Nystrom, T.; Hanstorp, D. A Microfluidic System in Combination with Optical Tweezers for Analyzing Rapid and Reversible Cytological Alterations in Single Cells upon Environmental Changes. *Lab Chip* **2007**, *7*, 71.

(13) Applegate, R. W., Jr.; Squier, J.; Vestad, T.; Oakey, J.; Marr, D. W. M. Optical Trapping, Manipulation, and Sorting of Cells and

Colloids in Microfluidic Systems with Diode Laser Bars. *Opt. Express* **2004**, *12*, 4390−4398.
(14) Neale, S. L.; MacDonald, M. P.; Dholakia, K.; Krauss, T. F. All-optical Control of Microfluidic Components using Form Birefringence. *Nat. Mater.* **2005**, *4*, 530−533.
(15) Juan, M. L.; Righini, M.; Quidant, R. Plasmon Nano-optical Tweezers. *Nat. Photonics* **2011**, *5*, 349−356.
(16) Kwak, E. S.; Onuta, T. D.; Amarie, D.; Potyrailo, R.; Stein, B.; Jacobson, S. C.; Schaich, W. L.; Dragnea, B. Optical Trapping with Integrated Near-Field Apertures. *J. Phys. Chem. B* **2004**, *108*, 13607.
(17) Righini, M.; Zelenina, A. S.; Girard, C.; Quidant, R. Parallel and Selective Trapping in a Patterned Plasmonic Landscape. *Nat. Phys.* **2007**, *3*, 477−480.
(18) Zhang, W.; Huang, L.; Santschi, C.; Martin, O. J. F. Trapping and Sensing 10 nm Metal Nanoparticles using Plasmonic Dipole Antennas. *Nano Lett.* **2010**, *10*, 1006−1011.
(19) Wang, K.; Schonbrun, E.; Steinvurzel, P.; Crozier, K. B. Trapping and Rotating Nanoparticles using a Plasmonic Nano-tweezer with an Integrated Heat Sink. *Nat. Commun.* **2011**, *2*, 469.
(20) Hansen, P.; Zheng, Y.; Ryan, J.; Hesselink, L. Nano-Optical Conveyor Belt, Part I: Theory. *Nano Lett.* **2014**, DOI: 10.1021/nl404011s.
(21) Shi, X.; Hesselink, L.; Thornton, R. Ultrahigh Light Transmission through a C-shaped Nanoaperture. *Opt. Lett.* **2003**, *28*, 1320.
(22) Vogel, N.; Zieleniecki, J.; Koper, I. As flat as it gets: Ultrasmooth Surfaces from Template-stripping Procedures. *Nanoscale* **2012**, *4*, 3820.
(23) Zhu, X.; Zhang, Y.; Zhang, J.; Xu, J.; Ma, Y.; Li, Z.; Yu, D. Ultrafine and Smooth Full Metal Nanostructures for Plasmonics. *Adv. Mater.* **2010**, *22*, 4345.